NANO LETTERS

pubs.acs.org/NanoLett Letter

Converting a Monolayered $NbSe_2$ into an Ising Superconductor with Nontrivial Band Topology via Physical or Chemical Pressuring

Leiqiang Li, Shunhong Zhang, Guojing Hu, Linhai Guo, Tong Wei, Wei Qin, Bin Xiang, Changgan Zeng, Zhenyu Zhang,* and Ping Cui*

Cite This: https://doi.org/10.1021/acs.nanolett.2c02422 Read Online

ACCESS | Metrics & More | Article Recommendations | Supporting Information

ABSTRACT: Two-dimensional transition metal dichalcogenides possessing superconductivity and strong spin−orbit coupling exhibit high in-plane upper critical fields due to Ising pairing. Yet to date, whether such systems can become topological Ising superconductors remains to be materialized. Here we show that monolayered $NbSe_2$ can be converted into Ising superconductors with nontrivial band topology via physical or chemical pressuring. Using first-principles calculations, we first demonstrate that a hydrostatic pressure higher than 2.5 GPa can induce a $p-d$ band inversion, rendering nontrivial band topology to $NbSe_2$. We then illustrate that Te-doping can function as chemical pressuring in inducing nontrivial topology in $NbSe_{2-x}Te_x$ with $x \geq 0.8$, due to a larger atomic radius and stronger spin−orbit coupling of Te. We also evaluate the upper critical fields within both approaches, confirming the enhanced Ising superconductivity nature, as experimentally observed. Our findings may prove to be instrumental in material realization of topological Ising superconductivity in two-dimensional systems.

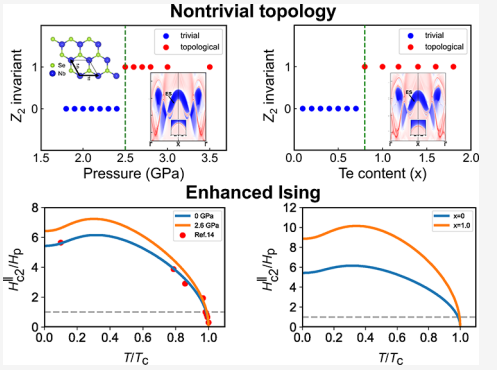

KEYWORDS: *Ising superconductivity, nontrivial topology, first-principles calculations, transition metal dichalcogenides, pressuring*

Over the past decade, transition metal dichalcogenides (TMDs)[1,2] have been actively explored as an attractive class of systems in the rapidly expanding two-dimensional (2D) materials family. These systems can be expressed as MX_2, where M represents a transition metal element and X represents a chalcogen element. Given the vast choices of M and variations in X, diverse physical properties can be harbored by the TMD materials. Furthermore, the inherently weak interlayer couplings in these systems offer another highly effective tuning knob to reveal their thickness-dependent properties down to the monolayer regime.[3] Recent striking examples include the predictions and observations of quantum spin Hall states in WTe_2,[4−7] superconductivity in $NbSe_2$,[8−10] and even potential realizations of topological superconductivity in WTe_2,[11,12] all achieved using monolayered systems. These advances, in turn, have substantially enriched our understandings of low-dimensional electron systems that exhibit globally nontrivial and/or macroscopic quantum behaviors.

Among the superconducting properties, Ising superconductivity has gained increasing attention since its first observations in TMD systems,[13−19] due to the surprisingly high in-plane upper critical fields ($H_{c2}^{\parallel}$) well above the Pauli paramagnetic limits.[20] The underlying mechanism is the effective Zeeman field, generated by the broken inversion symmetry in the few-layer regime, allowing the inherently strong spin−orbit coupling (SOC) of the systems to lock the spins of the electrons moving in-plane into the out-of-plane directions. Very recently, it has also been proposed that the conditions for Ising pairing can be further relaxed in the so-called type-II Ising systems, namely, without invoking the inversion symmetry breaking,[21] as experimentally demonstrated in different centrosymmetric systems.[22,23] Given the indispensable strong nature of SOC in Ising superconductors as well as the vital role of SOC in many topological materials, it is conceivable that topological Ising superconductivity may also emerge as a new property of quantum matter. Several theoretical efforts have been reported toward this goal,[24−26] yet to date a definitive materialization remains to be achieved.

In this Letter, we use first-principles approaches to unveil that a monolayered $NbSe_2$ as a representative Ising superconductor can be further enriched into an Ising superconductor with nontrivial band topology via physical or chemical pressuring. Specifically, we first show that a hydrostatic pressure over a critical value of 2.5 GPa can induce a $p-d$ band inversion in a $NbSe_2$ monolayer,

Received: June 20, 2022
Revised: August 1, 2022

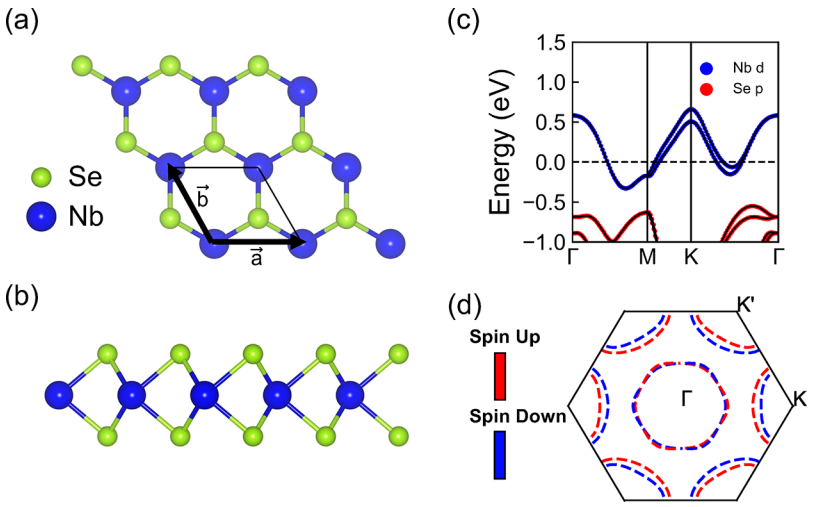

Figure 1. (a) Top and (b) side views of the crystal structure of 1*H*-$NbSe_2$, with the unit cell highlighted by the black solid lines and lattice vectors ($\vec{a}$ and $\vec{b}$) shown in (a). (c) Orbital- and element-resolved band structure of 1*H*-$NbSe_2$ with the SOC. The Fermi level is set at zero. (d) Spin-projected Fermi surface of 1*H*-$NbSe_2$.

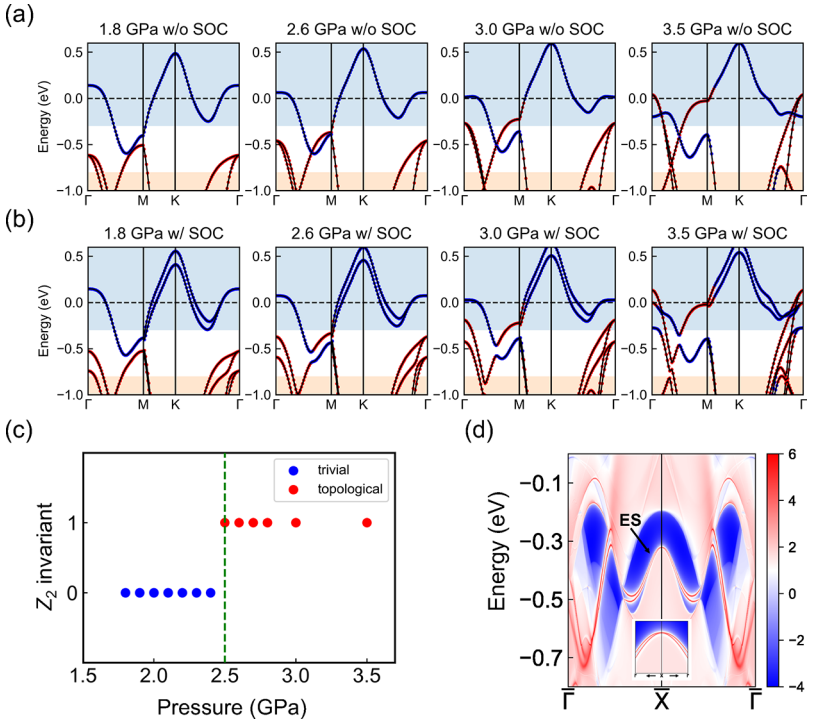

Figure 2. Band structures of 1*H*-$NbSe_2$ at 1.8, 2.6, 3.0, and 3.5 GPa (a) without and (b) with the SOC. The blue and red data points denote the spectral weights contributed by the Nb-*d* and Se-*p* orbitals, respectively. The Fermi levels are all set at zero. (c) Calculated Z_2 invariants for 1*H*-$NbSe_2$ under different pressures. (d) Edge states (ES) of the semi-infinite slab along an Se-terminated Nb-zigzag edge at 3.0 GPa, with its Dirac nature at the $\bar{X}$ point as highlighted in the inset. The warmer colors denote higher local density of states, and the blue regions denote the bulk band gaps.

introducing a topological phase transition ($Z_2 = 1$) to the system while still preserving its superconducting property. Next, we demonstrate that substitution of Se by Te can function as an even more superior approach of chemical pressuring in inducing the nontrivial $p-d$ band inversion in an alloyed monolayer of $NbSe_{2-x}Te_x$ when $x \geq 0.8$, originating from the dual effects of a larger atomic radius and stronger SOC of Te. We also evaluate the in-plane upper critical fields at different pressures or doping concentrations and confirm the enhanced Ising superconductivity nature. Encouragingly, we have further carried out preliminary experimental studies to confirm that the $NbSe_{2-x}Te_x$ samples indeed exhibit enhanced Ising superconductivity. Collectively, the central findings presented here offer appealing new approaches toward definitive materialization of topological Ising superconductivity in 2D systems.

Monolayered $NbSe_2$ and Design Principle. As displayed in Figure 1a,b, monolayered $NbSe_2$ with the *H* phase (labeled as 1*H*-$NbSe_2$) exhibits the same trigonal prismatic cage as that for its bulk counterpart,[27] though the symmetry is reduced to $P\bar{6}m2$ (D_{3h}^1) because of the broken inversion symmetry. Our density functional theory (DFT) calculations

https://doi.org/10.1021/acs.nanolett.2c02422
Nano Lett. XXXX, XXX, XXX−XXX

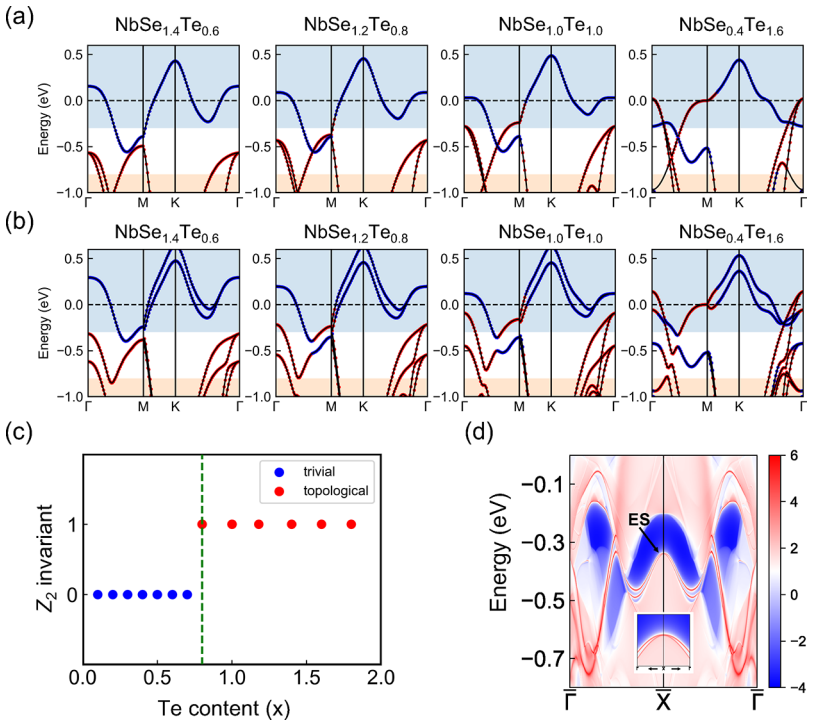

Figure 3. Band structures of 1*H*-$NbSe_{2-x}Te_x$ with x = 0.6, 0.8, 1.0, and 1.6 (a) without and (b) with the SOC. The blue and red data points denote the spectral weights contributed by the Nb-*d* and Se(Te)-*p* orbitals, respectively. (c) Calculated Z_2 invariants for 1*H*-$NbSe_{2-x}Te_x$ at increasing Te contents. (d) Edge states (ES) of the semi-infinite slab along an Se-terminated Nb-zigzag edge for x = 1.0, with its Dirac nature at the $\bar{X}$ point as highlighted in the inset.

show that 1*H*-$NbSe_2$ is the most stable phase, with the lattice constants $a = b$ = 3.454 Å.[28] Figure 1c,d displays the electronic structures of 1*H*-$NbSe_2$ obtained with the SOC. The system is metallic, consistent with the observations of its superconducting properties.[8,14,18] The Fermi surface, mainly contributed by the Nb-*d* orbitals, possesses a cylindrical hole pocket at the Γ point, while the valence bands right below the Fermi level mainly originate from the Se-*p* orbitals. The gap between the Nb-*d* and Se-*p* bands is about 0.2 eV, which can be readily manipulated to induce the necessary band inversion. The lack of an inversion symmetry and presence of the SOC lead to the opposite spin splittings around the K (K′) points shown in Figure 1d, and the resultant effective Zeeman field pins the electron spins to the out-of-plane directions, rendering the Ising pairing nature to the system.[14,18]

To potentially realize topological Ising superconductivity in 1*H*-$NbSe_2$, our main design principle is that pressuring can effectively narrow the band gap down to a critical value or even close it, enabling the SOC to further hybridize the relevant bands and open an inverted gap at proper high-symmetry point(s) in *k*-space, thereby resulting in a topological phase transition. One natural way of pressuring is to apply hydrostatic pressure. Another way is via substitutional doping with a foreign element of a different atomic radius, which can be viewed as applying a chemical pressure. Both pressuring approaches are explored to tune the electronic structures of monolayered $NbSe_2$. In particular, to largely preserve the main band feature of $NbSe_2$, substitutional doping of Se by Te is chosen. Because Te possesses a larger atomic radius and stronger SOC, this chemical pressuring is expected to function as an even more appealing way to induce nontrivial band topology than physical pressuring, as the stronger SOC is also favorable for the preservation or enhancement of the Ising pairing. Both pressuring approaches may convert the systems into topological Ising superconductors.

Physical Pressuring Effect on Band Topology. First, we explore the effects of a hydrostatic pressure on the band structures of monolayered $NbSe_2$. Our calculations show that the 1*H* phase is always energetically more stable than the 1*T* phase within the pressure range considered in this study, confirming no structural phase transition. The corresponding band structures without or with the SOC under different pressures are displayed in Figures 2a,b and S1. The Nb-*d* and Se-*p* bands are moving closer toward each other with increasing pressure, especially along the Γ-M path in the first Brillouin zone. As shown in Figure 2a, at 1.8 GPa, the bands first touch and then cross upon increasing pressure. Here, the underlying physical reason is that the hydrostatic pressure compresses the lattice constants and shortens the bond lengths, leading to more dispersive band structures and band gap closing. In particular, when the pressure reaches 2.5 GPa or higher, the Se-*p* bands have moved to be essentially degenerate with or higher than the Nb-*d* bands at the M points. With the SOC included, the crossing bands open a gap, associated with an explicit inversion of their orbital contributions (see Figure 2b). If the pressure continues to increase, inverted band orders also exist at the Γ point, e.g., at 3.5 GPa. Such *p*−*d* band inversions at the high-symmetry points may result in a topological phase transition, as examined later.

Given the above analysis on the band inversion of 1*H*-$NbSe_2$ under varying pressure, we now determine the topological properties by evaluating the topological invariant Z_2. In doing so, we stress that, even though the systems have no global band gap, there exist well-defined curved chemical potentials between the relevant inverted bands, separating the bands

https://doi.org/10.1021/acs.nanolett.2c02422
Nano Lett. XXXX, XXX, XXX−XXX

Table 1. Calculated Superconducting Transition Temperature (T_c), Spin Splitting Energy (Δ_{so}), and Ising Spin-Orbit Field (H_{so}) under Different Physical Pressures (P) or Te Doping Contents (x)

	P (GPa)					
	0.6	1.8	2.4	2.6	3.0	3.5
T_c (K)	3.36	3.53	3.16	3.22	4.07	4.12
Δ_{so} (meV)	71.7	79.8	82.7	83.3	84.7	86.1
H_{so} (T)	619.6	691.0	714.4	719.5	731.8	743.3
	x					
	0.4	0.6	0.8	1.0	1.4	1.6
Δ_{so} (meV)	82.9	91.4	98.9	104.6	113.4	116.5
H_{so} (T)	717.0	789.2	854.1	903.4	979.3	1006.0

into "occupied" and "unoccupied" states (see section S3). The corresponding Z_2 invariant is determined by the "occupied" states, as calculated by following the Wannier charge center method.[29] Such an approach in identifying the band topology has been employed in studying $FeSe_{0.5}Te_{0.5}$,[30] and the robust topological superconductivity thus predicted has been further confirmed experimentally.[31−34] The calculated Z_2 invariants under different pressures are summarized in Figure 2c, establishing a critical pressure of 2.5 GPa, above which the monolayered $NbSe_2$ is in the topologically nontrivial phase with $Z_2 = 1$. It should be emphasized that the nontrivial topology of the systems is solely determined by the band inversion at the M points. In particular, at 3.5 GPa, the band inversion at the Γ point takes place below the curved chemical potential (see Figure 2b), which does not contribute to the topological phase transition. As another manifestation of the nontrivial topology in the band structures, the edge states of a semi-infinite slab along an Se-terminated Nb-zigzag edge of $NbSe_2$ at 3.0 GPa are shown in Figures 2d and S3, with the Dirac nature at the $\bar{X}$ point highlighted. The energy spectra for a semi-infinite slab of $NbSe_2$ with increasing pressure are also presented in Figure S4, demonstrating the evolution of the edge states from the trivial to nontrivial regime.

It is noted that the structural reconstructions caused by the charge density wave (CDW) phase transition have been reported in 1H-$NbSe_2$.[8,16,35,36] Here we further investigate the effects of the CDW on the electronic and topological properties by considering two energetically degenerate 3 × 3 CDW structures of 1H-$NbSe_2$ (see section S5). We find the band structures exhibit similar characteristics to that of the non-CDW phase, and the corresponding band topologies also stay intact. We do not expect the CDW phases under physical pressuring to influence the electronic and topological properties of the systems either.

Chemical Pressuring Effect on Band Topology. Next, we investigate how chemical pressuring can function as another appealing approach in inducing the nontrivial p−d band inversion by introducing Te substitutional doping to 1H-$NbSe_2$. To do so, we have first confirmed that the 1H phase remains to be energetically stable for $NbSe_{2-x}Te_x$ with $x = 0$−2 (see Table S1). In particular, when $x = 2$, the system still slightly prefers the 1H phase than the 1T phase.

To analyze the electronic properties of $NbSe_{2-x}Te_x$ with an arbitrary Te doping concentration, the virtual crystal approximation (VCA) method[37,38] has been adopted. Figure 3a,b shows the projected band structures of $NbSe_{2-x}Te_x$ with x = 0.6, 0.8, 1.0, and 1.6 without and with the SOC, respectively, exhibiting similar trends in the band evolution as observed when applying a hydrostatic pressure. Specifically, when $x \geq$ 0.8, the Se-p bands have moved to be essentially degenerate with or higher than the Nb-d bands at the M points; when $x >$ 1.2, inverted band orders also exist at the Γ point (see Figure S6). Such band inversions are again likely to result in a topological phase transition.

Using the "curved chemical potential" approach, we further calculate the Z_2 invariants to identify the potential topological properties of the $NbSe_{2-x}Te_x$ at different x. As shown in Figure 3c, when $x \geq 0.8$, the system hosts a topologically nontrivial phase with $Z_2 = 1$. Similar to the case of 3.5 GPa, when $x > 1.2$, the band inversions at the Γ point (Figure 3b) do not actually contribute to the topological phase transition of the system. Instead, its nontrivial topology is again solely determined by the band inversion at the M points. As a reflection of the bulk-surface correspondence, the topologically protected nontrivial edge states for $x = 1.0$ are also displayed in Figure 3d. In addition, our selective test calculations based on the unfolding method[39] using the 2 × 2 supercells also yield similar characteristics in the band structures and identical band topology as from the VCA approach (see section S7), verifying the general validity of the VCA method.

Enhanced Ising Superconductivity in $NbSe_2$. With the nontrivial band topology confirmed above under physical or chemical pressuring, we now need to examine individually whether the superconducting property and Ising nature of pairing can still be preserved under such conditions. Here, we first focus on the superconducting aspect. Using the standard Eliashberg formalism,[40−42] we estimate the superconducting transition temperature (T_c) of 1H-$NbSe_2$ to be 3.0 K (see section S8), consistent with the values measured experimentally.[14,18] The phonon dispersions of $NbSe_2$ under different pressures are shown in Figure S8, and the corresponding pressure-dependent T_c's are listed in Table 1, all of which showing relatively small variations from that under no pressure. As for the Te-doped systems, we cannot readily obtain T_c at an arbitrary x within the VCA scheme. Instead, we have checked the high-symmetry case of $x = 1$ (namely, 1H-NbSeTe) using the standard supercell method and obtained $T_c = 2.30$ K. Qualitatively, such T_c reduction is consistent with our preliminary experimental results using flake samples (see section S11). We therefore conclude that the superconducting property of 1H-$NbSe_2$ can be well preserved upon the application of a proper hydrostatic or chemical pressure. Here it is noted that we have also examined the multigap features of these systems by solving the anisotropic Migdal−Eliashberg formalism,[43] and more discussions (including the CDW effects on T_c) are presented in section S9.

Next, we investigate the Ising pairing aspect of the systems, to ensure that the pressuring induced topological phase

https://doi.org/10.1021/acs.nanolett.2c02422
Nano Lett. XXXX, XXX, XXX−XXX

transition will not compromise the Ising nature reflected by the exceptionally high in-plane upper critical field. In doing so, we calculate $H_{c2}^{\parallel}$ via an established microscopic model based on the Gor'kov Green function technique, in which the superconductivity is protected by Zeeman-type spin−orbit interaction with Rashba spin−orbit interaction,[22,44]

$$\ln\left(\frac{T}{T_c}\right) + \frac{1}{2}\left[1 - \frac{2(\widetilde{\alpha_R k_F})^2 + \tilde{\beta}_{so}^{\ 2} - \mu_B^{\ 2} H_{c2}^{\parallel 2}}{\rho_+^{\ 2} - \rho_-^{\ 2}}\right] \times \mathrm{Re}\left[\psi\left(\frac{1}{2} + \frac{i\rho_+}{2\pi k_B T}\right) - \psi\left(\frac{1}{2}\right)\right] + \frac{1}{2}\left[1 + \frac{2(\widetilde{\alpha_R k_F})^2 + \tilde{\beta}_{so}^{\ 2} - \mu_B^{\ 2} H_{c2}^{\parallel 2}}{\rho_+^{\ 2} - \rho_-^{\ 2}}\right] \times \mathrm{Re}\left[\psi\left(\frac{1}{2} + \frac{i\rho_-}{2\pi k_B T}\right) - \psi\left(\frac{1}{2}\right)\right] = 0 \quad (1)$$

where

$$2\rho_{\pm} = \sqrt{(\mu_B H_{c2}^{\parallel} + \widetilde{\alpha_R k_F})^2 + (\widetilde{\alpha_R k_F})^2 + \tilde{\beta}_{so}^{\ 2}} \pm \sqrt{(\mu_B H_{c2}^{\parallel} - \widetilde{\alpha_R k_F})^2 + (\widetilde{\alpha_R k_F})^2 + \tilde{\beta}_{so}^{\ 2}},$$

$\tilde{\beta}_{so} = \Delta_{so}/[1 + \hbar/(2\pi k_B T_c \tau)]$ is the effective Zeeman-type splitting energy, $\widetilde{\alpha_R k_F} = \alpha_R k_F/\sqrt{2}[1 + \hbar(2\pi k_B T_c \tau)]$ is the effective Rashba-type splitting energy, τ is the spin−orbit scattering time, T is the superconducting transition temperature in the presence of an in-plane magnetic field, $\psi(x)$ is the digamma function, μ_B is the Bohr magneton, κ_B is the Boltzmann constant, and Δ_{so} measures the spin splitting energy averaged over the Fermi surface in the first Brillouin zone.[14,18] Based on the spin-projected Fermi surface shown in Figure 1d, we obtain Δ_{so} = 68 meV for the monolayered $NbSe_2$ and the corresponding Ising spin−orbit field H_{so} is $\Delta_{so}/2\mu_B$ = 586.5 T, consistent with previous studies.[14,18] The spin-projected Fermi surfaces for 1*H*-$NbSe_2$ under varying pressure are shown in Figure 4a. We notice that the spin splitting is enlarged upon increasing pressure, and the corresponding Δ_{so} are presented in Table 1, showing again its increasing tendency.

According to eq 1, we further gain the evolution of the in-plane upper critical field with the transition temperature. First, we use eq 1 to fit the experimental data for the $NbSe_2$ monolayer, including the data extracted from Figure 4 in ref 14 and $H_{c2}^{\parallel}$ = 31.5 at T = 0.3 K in the Supporting Information of ref 14, which yields $\tilde{\beta}_{so}$ = 8.77 meV, $\widetilde{\alpha_R k_F}$ = 0.58 meV, and τ = 60 fs (see Figure 4c). We then use the same τ and $\widetilde{\alpha_R k_F}$ to further estimate the $H_{c2}^{\parallel}$ at different pressures, as shown in Figures 4c and S10, confirming that $H_{c2}^{\parallel}/H_p \gg 1$, where H_p is the Pauli paramagnetic limit.[20] Therefore, the Ising pairing nature of the system is well preserved under hydrostatic pressures. It is noted that we have also employed a pair breaking equation[45,46] to estimate the evolution of $H_{c2}^{\parallel}$ with the transition temperature, as done in the first demonstration of the $NbSe_2$ monolayer as an Ising superconductor,[14] and the similar Ising pairing nature is obtained under hydrostatic pressures (see section S10).

To finally verify the Ising nature of the monolayered $NbSe_{2-x}Te_x$, we have also examined the doping effect on the

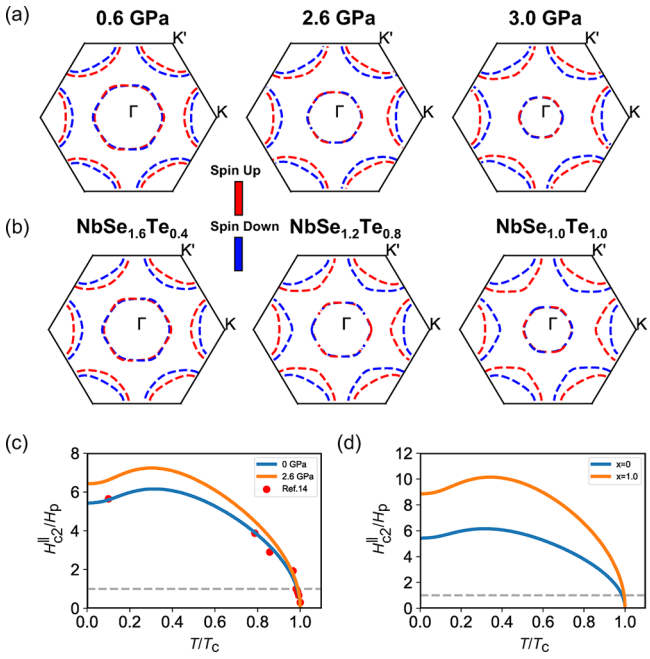

Figure 4. (a) Evolutions of the spin-projected Fermi surfaces for 1*H*-$NbSe_2$ at 0.6, 2.6, and 3.0 GPa. (b) Same as (a) but for 1*H*-$NbSe_{2-x}Te_x$ at x = 0.4, 0.8, and 1.0. (c) In-plane upper critical field $H_{c2}^{\parallel}$ as a function of the transition temperature T for 1*H*-$NbSe_2$ at 0 and 2.6 GPa, both in reduced units as described in the main text. (d) Same as (c) but for 1*H*-$NbSe_{2-x}Te_x$ at x = 0 and 1.0. The red dots represent the experimental data extracted from ref 14.

spin splittings of the Fermi surfaces. In Figure 4b, we can see that Δ_{so} enlarges explicitly with the increasing Te content. By using the same τ and $\widetilde{\alpha_R k_F}$ as that for 1*H*-$NbSe_2$, the $H_{c2}^{\parallel}/H_p$ versus T/T_c plot at x = 1 is shown in Figure 4d, revealing distinctly enhanced $H_{c2}^{\parallel}$ from that of the undoped 1*H*-$NbSe_2$. Such more pronounced spin splittings and further enhanced $H_{c2}^{\parallel}$ result from the dual effects of the Te dopants, namely, the pressure effect associated with their larger atomic radius and the stronger SOC. Therefore, the Ising pairing nature of 1*H*-$NbSe_2$ is also well preserved (in fact substantially enhanced) within the chemical pressuring approach.

Discussion. Before closing, we briefly discuss the experimental feasibility aspects of the present study. First, applying a physical pressure has been established as a powerful route to modulate electronic properties of materials,[47−49] suggesting that our proposal based on a hydrostatic pressure can be verified in future experiments. Second, when a substrate is inevitable, substrates with weak interfacial coupling are preferred, such as bilayer graphene (BLG)/SiC(0001), which has been proven to be weakly coupled to the $NbSe_2$ overlayers.[10,14,16,50] Third, substitutional doping of atoms in compound materials has also been well established, including the TMD systems.[51−53] In particular, the superconducting NbSeTe bulk material has recently been successfully synthesized, showing $T_c \sim$ 1.3 K.[54] Even more encouragingly, motivated by the present predictions, we have further carried out preliminary studies to fabricate the $NbSe_{2-x}Te_x$ samples and characterize the superconducting properties of the mechanically exfoliated flakes under different magnetic fields (see more details in section S11). Such flakes indeed exhibit both persistent superconductivity and substantially enhanced Ising pairing for a broad range of Te concentrations, especially

https://doi.org/10.1021/acs.nanolett.2c02422
Nano Lett. XXXX, XXX, XXX−XXX

including the Te-doping levels predicted to achieve nontrivial band topology. Fourth, the existence of the edge states in the present systems can be signified by the enhanced intensity of the local density of states at the sample edges in a proper energy window (see also Figure S17), as recently demonstrated using scanning tunneling spectroscopy for related systems.[55−58] Finally, if the topological edge bands disperse upward to the Fermi level, such topological states can directly participate in the superconducting pairing. Even if they are located below the Fermi level, it is still feasible to participate in the superconducting pairing under proper carrier doping or gating.[59]

In conclusion, we have identified that monolayered $NbSe_2$ can be converted into an Ising superconductor with nontrivial band topology via physical or chemical pressuring. Our calculations have demonstrated that a hydrostatic pressure over 2.5 GPa or substitution of Se by Te to form alloyed $NbSe_{2-x}Te_x$ with $x \geq 0.8$ can induce $p-d$ band inversions, rendering nontrivial topology to the $NbSe_2$ systems. Meanwhile, the superconducting and Ising properties of these systems are well preserved. In particular, the Ising paring nature in the Te-doped systems has been explicitly enhanced, as signified by the significantly enhanced in-plane upper critical fields over the monolayered $NbSe_2$, also as experimentally confirmed. Collectively, our central findings provide crucial new pathways toward material realization of topological Ising superconductivity in 2D systems.

■ ASSOCIATED CONTENT

Supporting Information

The Supporting Information is available free of charge at https://pubs.acs.org/doi/10.1021/acs.nanolett.2c02422.

Computational methods, band proximity effect, T_c estimation, preliminary experimental results on fabrication and superconductivity characterization of the $NbSe_{2-x}Te_x$ samples, and supporting figures and table (PDF)

■ AUTHOR INFORMATION

Corresponding Authors

Zhenyu Zhang − *International Center for Quantum Design of Functional Materials (ICQD), and CAS Center for Excellence in Quantum Information and Quantum Physics, University of Science and Technology of China, Hefei, Anhui 230026, China; Hefei National Laboratory, University of Science and Technology of China, Hefei 230088, China;* orcid.org/0000-0001-5844-3558; Email: zhangzy@ustc.edu.cn

Ping Cui − *International Center for Quantum Design of Functional Materials (ICQD), and CAS Center for Excellence in Quantum Information and Quantum Physics, University of Science and Technology of China, Hefei, Anhui 230026, China; Hefei National Laboratory, University of Science and Technology of China, Hefei 230088, China;* orcid.org/0000-0003-3196-2563; Email: cuipg@ustc.edu.cn

Authors

Leiqiang Li − *International Center for Quantum Design of Functional Materials (ICQD), and CAS Center for Excellence in Quantum Information and Quantum Physics, University of Science and Technology of China, Hefei, Anhui 230026, China;* orcid.org/0000-0002-1754-1466

Shunhong Zhang − *International Center for Quantum Design of Functional Materials (ICQD), and CAS Center for Excellence in Quantum Information and Quantum Physics, University of Science and Technology of China, Hefei, Anhui 230026, China;* orcid.org/0000-0003-2120-4574

Guojing Hu − *Department of Materials Science & Engineering, CAS Key Lab of Materials for Energy Conversion, Anhui Laboratory of Advanced Photon Science and Technology, University of Science and Technology of China, Hefei, Anhui 230026, China*

Linhai Guo − *International Center for Quantum Design of Functional Materials (ICQD), and CAS Center for Excellence in Quantum Information and Quantum Physics, University of Science and Technology of China, Hefei, Anhui 230026, China*

Tong Wei − *International Center for Quantum Design of Functional Materials (ICQD), and CAS Center for Excellence in Quantum Information and Quantum Physics, University of Science and Technology of China, Hefei, Anhui 230026, China*

Wei Qin − *Department of Physics, The University of Texas at Austin, Austin, Texas 78712, United States;* orcid.org/0000-0003-1035-1130

Bin Xiang − *Department of Materials Science & Engineering, CAS Key Lab of Materials for Energy Conversion, Anhui Laboratory of Advanced Photon Science and Technology, University of Science and Technology of China, Hefei, Anhui 230026, China; Hefei National Laboratory, University of Science and Technology of China, Hefei 230088, China;* orcid.org/0000-0001-8254-8640

Changgan Zeng − *International Center for Quantum Design of Functional Materials (ICQD), and CAS Center for Excellence in Quantum Information and Quantum Physics, University of Science and Technology of China, Hefei, Anhui 230026, China; Hefei National Laboratory, University of Science and Technology of China, Hefei 230088, China;* orcid.org/0000-0001-8630-845X

Complete contact information is available at: https://pubs.acs.org/10.1021/acs.nanolett.2c02422

Notes

The authors declare no competing financial interest.

■ ACKNOWLEDGMENTS

This work was supported by the Innovation Program for Quantum Science and Technology (Grant No. 2021ZD0302800), the National Natural Science Foundation of China (Grant Nos. 11634011, 11722435, 11974323, and 11904350), the National Key R&D Program of China (Grant No. 2017YFA0303500), the Anhui Initiative in Quantum Information Technologies (Grant No. AHY170000), and the Strategic Priority Research Program of Chinese Academy of Sciences (Grant No. XDB30000000).

■ REFERENCES

(1) Mak, K. F.; Lee, C.; Hone, J.; Shan, J.; Heinz, T. F. Atomically thin MoS_2: a new direct-gap semiconductor. *Phys. Rev. Lett.* **2010**, *105*, 136805.

(2) Xu, X.; Yao, W.; Xiao, D.; Heinz, T. F. Spin and pseudospins in layered transition metal dichalcogenides. *Nat. Phys.* **2014**, *10*, 343−350.

(3) Radisavljevic, B.; Radenovic, A.; Brivio, J.; Giacometti, V.; Kis, A. Single-layer MoS_2 transistors. *Nat. Nanotechnol.* **2011**, *6*, 147−150.
(4) Qian, X.; Liu, J.; Fu, L.; Li, J. Quantum spin Hall effect in two-dimensional transition metal dichalcogenides. *Science* **2014**, *346*, 1344−1347.
(5) Fei, Z.; Palomaki, T.; Wu, S.; Zhao, W.; Cai, X.; Sun, B.; Nguyen, P.; Finney, J.; Xu, X.; Cobden, D. H. Edge conduction in monolayer WTe_2. *Nat. Phys.* **2017**, *13*, 677−682.
(6) Tang, S.; Zhang, C.; Wong, D.; Pedramrazi, Z.; Tsai, H.-Z.; Jia, C.; Moritz, B.; Claassen, M.; Ryu, H.; Kahn, S.; Jiang, J.; Yan, H.; Hashimoto, M.; Lu, D.; Moore, R. G.; Hwang, C.-C.; Hwang, C.; Hussain, Z.; Chen, Y.; Ugeda, M. M.; Liu, Z.; Xie, X.; P. Devereaux, T.; Crommie, M. F.; Mo, S.-K.; Shen, Z.-X. Quantum spin Hall state in monolayer 1T'-WTe_2. *Nat. Phys.* **2017**, *13*, 683−687.
(7) Wu, S.; Fatemi, V.; Gibson, Q. D.; Watanabe, K.; Taniguchi, T.; Cava, R. J.; Jarillo-Herrero, P. Observation of the quantum spin Hall effect up to 100 K in a monolayer crystal. *Science* **2018**, *359*, 76−79.
(8) Ugeda, M. M.; Bradley, A. J.; Zhang, Y.; Onishi, S.; Chen, Y.; Ruan, W.; Ojeda-Aristizabal, C.; Ryu, H.; Edmonds, M. T.; Tsai, H.-Z.; Riss, A.; Mo, S.-K.; Lee, D.; Zettl, A.; Hussain, Z.; Shen, Z.-X.; Crommie, M. F. Characterization of collective ground states in single-layer $NbSe_2$. *Nat. Phys.* **2016**, *12*, 92−97.
(9) Saito, Y.; Nojima, T.; Iwasa, Y. Highly crystalline 2D superconductors. *Nat. Rev. Mater.* **2017**, *2*, 16094.
(10) Zhao, K.; Lin, H.; Xiao, X.; Huang, W.; Yao, W.; Yan, M.; Xing, Y.; Zhang, Q.; Li, Z.-X.; Hoshino, S.; Wang, J.; Zhou, S.; Gu, L.; Bahramy, M. S.; Yao, H.; Nagaosa, N.; Xue, Q.-K.; Law, K. T.; Chen, X.; Ji, S.-H. Disorder-induced multifractal superconductivity in monolayer niobium dichalcogenides. *Nat. Phys.* **2019**, *15*, 904−910.
(11) Sajadi, E.; Palomaki, T.; Fei, Z.; Zhao, W.; Bement, P.; Olsen, C.; Luescher, S.; Xu, X.; Folk, J. A.; Cobden, D. H. Gate-induced superconductivity in a monolayer topological insulator. *Science* **2018**, *362*, 922−925.
(12) Fatemi, V.; Wu, S.; Cao, Y.; Bretheau, L.; Gibson, Q. D.; Watanabe, K.; Taniguchi, T.; Cava, R. J.; Jarillo-Herrero, P. Electrically tunable low-density superconductivity in a monolayer topological insulator. *Science* **2018**, *362*, 926−929.
(13) Lu, J.; Zheliuk, O.; Leermakers, I.; Yuan, N. F.; Zeitler, U.; Law, K. T.; Ye, J. Evidence for two-dimensional Ising superconductivity in gated MoS_2. *Science* **2015**, *350*, 1353−1357.
(14) Xi, X.; Wang, Z.; Zhao, W.; Park, J.-H.; Law, K. T.; Berger, H.; Forró, L.; Shan, J.; Mak, K. F. Ising pairing in superconducting $NbSe_2$ atomic layers. *Nat. Phys.* **2016**, *12*, 139−143.
(15) Saito, Y.; Nakamura, Y.; Bahramy, M. S.; Kohama, Y.; Ye, J.; Kasahara, Y.; Nakagawa, Y.; Onga, M.; Tokunaga, M.; Nojima, T.; Yanase, Y.; Iwasa, Y. Superconductivity protected by spin−valley locking in ion-gated MoS_2. *Nat. Phys.* **2016**, *12*, 144−149.
(16) Xing, Y.; Zhao, K.; Shan, P.; Zheng, F.; Zhang, Y.; Fu, H.; Liu, Y.; Tian, M.; Xi, C.; Liu, H.; Feng, J.; Lin, X.; Ji, S.-H.; Chen, X.; Xue, Q.-K.; Wang, J. Ising superconductivity and quantum phase transition in macro-size monolayer $NbSe_2$. *Nano Lett.* **2017**, *17*, 6802−6807.
(17) Lu, J.; Zheliuk, O.; Chen, Q.; Leermakers, I.; Hussey, N. E.; Zeitler, U.; Ye, J. Full superconducting dome of strong Ising protection in gated monolayer WS_2. *Proc. Natl. Acad. Sci. U.S.A.* **2018**, *115*, 3551−3556.
(18) de la Barrera, S. C.; Sinko, M. R.; Gopalan, D. P.; Sivadas, N.; Seyler, K. L.; Watanabe, K.; Taniguchi, T.; Tsen, A. W.; Xu, X.; Xiao, D.; Hunt, B. M. Tuning Ising superconductivity with layer and spin−orbit coupling in two-dimensional transition-metal dichalcogenides. *Nat. Commun.* **2018**, *9*, 1427.
(19) Xing, Y.; Yang, P.; Ge, J.; Yan, J.; Luo, J.; Ji, H.; Yang, Z.; Li, Y.; Wang, Z.; Liu, Y.; Yang, F.; Qiu, P.; Xi, C.; Tian, M.; Liu, Y.; Lin, X.; Wang, J. Extrinsic and intrinsic anomalous metallic states in transition metal dichalcogenide Ising superconductors. *Nano Lett.* **2021**, *21*, 7486−7494.
(20) Clogston, A. M. Upper limit for the critical field in hard superconductors. *Phys. Rev. Lett.* **1962**, *9*, 266−267.
(21) Wang, C.; Lian, B.; Guo, X.; Mao, J.; Zhang, Z.; Zhang, D.; Gu, B.-L.; Xu, Y.; Duan, W. Type-II Ising superconductivity in two-dimensional materials with spin-orbit coupling. *Phys. Rev. Lett.* **2019**, *123*, 126402.
(22) Falson, J.; Xu, Y.; Liao, M.; Zang, Y.; Zhu, K.; Wang, C.; Zhang, Z.; Liu, H.; Duan, W.; He, K.; Liu, H.; Smet, J. H.; Zhang, D.; Xue, Q.-K. Type-II Ising pairing in few-layer stanene. *Science* **2020**, *367*, 1454−1457.
(23) Liu, Y.; Xu, Y.; Sun, J.; Liu, C.; Liu, Y.; Wang, C.; Zhang, Z.; Gu, K.; Tang, Y.; Ding, C.; Liu, H.; Yao, H.; Lin, X.; Wang, L.; Xue, Q.-K.; Wang, J. Type-II Ising superconductivity and anomalous metallic state in macro-size ambient-stable ultrathin crystalline films. *Nano Lett.* **2020**, *20*, 5728−5734.
(24) Zhou, B. T.; Yuan, N. F.; Jiang, H.-L.; Law, K. T. Ising superconductivity and Majorana fermions in transition-metal dichalcogenides. *Phys. Rev. B* **2016**, *93*, No. 180501R.
(25) Sharma, G.; Tewari, S. Yu-Shiba-Rusinov states and topological superconductivity in Ising paired superconductors. *Phys. Rev. B* **2016**, *94*, 094515.
(26) He, W.-Y.; Zhou, B. T.; He, J. J.; Yuan, N. F.; Zhang, T.; Law, K. T. Magnetic field driven nodal topological superconductivity in monolayer transition metal dichalcogenides. *Commun. Phys.* **2018**, *1*, 40.
(27) Liu, G.-B.; Xiao, D.; Yao, Y.; Xu, X.; Yao, W. Electronic structures and theoretical modelling of two-dimensional group-VIB transition metal dichalcogenides. *Chem. Soc. Rev.* **2015**, *44*, 2643−2663.
(28) Mattheiss, L. F. Band structures of transition-metal-dichalcogenide layer compounds. *Phys. Rev. B* **1973**, *8*, 3719−3740.
(29) Soluyanov, A. A.; Vanderbilt, D. Computing topological invariants without inversion symmetry. *Phys. Rev. B* **2011**, *83*, 235401.
(30) Wang, Z.; Zhang, P.; Xu, G.; Zeng, L.; Miao, H.; Xu, X.; Qian, T.; Weng, H.; Richard, P.; Fedorov, A. V.; Ding, H.; Dai, X.; Fang, Z. Topological nature of the $FeSe_{0.5}Te_{0.5}$ superconductor. *Phys. Rev. B* **2015**, *92*, 115119.
(31) Yin, J.-X.; Wu, Z.; Wang, J.; Ye, Z.; Gong, J.; Hou, X.; Shan, L.; Li, A.; Liang, X.; Wu, X.; Li, J.; Ting, C.-S.; Wang, Z.-Q.; Hu, J.-P.; Hor, P.-H.; Ding, H.; Pan, S. H. Observation of a robust zero-energy bound state in iron-based superconductor Fe(Te, Se). *Nat. Phys.* **2015**, *11*, 543−546.
(32) Zhang, P.; Yaji, K.; Hashimoto, T.; Ota, Y.; Kondo, T.; Okazaki, K.; Wang, Z.; Wen, J.; Gu, G.; Ding, H.; Shin, S. Observation of topological superconductivity on the surface of an iron-based superconductor. *Science* **2018**, *360*, 182−186.
(33) Wang, D.; Kong, L.; Fan, P.; Chen, H.; Zhu, S.; Liu, W.; Cao, L.; Sun, Y.; Du, S.; Schneeloch, J.; Zhong, R.; Gu, G.; Fu, L.; Ding, H.; Gao, H.-J. Evidence for Majorana bound states in an iron-based superconductor. *Science* **2018**, *362*, 333−335.
(34) Zhu, S.; Kong, L.; Cao, L.; Chen, H.; Papaj, M.; Du, S.; Xing, Y.; Liu, W.; Wang, D.; Shen, C.; Yang, F.; Schneeloch, J.; Zhong, R.; Gu, G.; Fu, L.; Zhang, Y.-Y.; Ding, H.; Gao, H.-J. Nearly quantized conductance plateau of vortex zero mode in an iron-based superconductor. *Science* **2020**, *367*, 189−192.
(35) Xi, X.; Zhao, L.; Wang, Z.; Berger, H.; Forró, L.; Shan, J.; Mak, K. F. Strongly enhanced charge-density-wave order in monolayer $NbSe_2$. *Nat. Nanotechnol.* **2015**, *10*, 765−769.
(36) Dreher, P.; Wan, W.; Chikina, A.; Bianchi, M.; Guo, H.; Harsh, R.; Mañínez-Galera, A. J.; Hofmann, P.; Miwa, J. A.; Ugeda, M. M.; et al. Proximity effects on the charge density wave order and superconductivity in single-layer $NbSe_2$. *ACS Nano* **2021**, *15*, 19430−19438.
(37) Mitchell, D. L.; Wallis, R. F. Theoretical energy-band parameters for the lead salts. *Phys. Rev.* **1966**, *151*, 581−595.
(38) Kriechbaum, M.; Ambrosch, K.; Fantner, E.; Clemens, H.; Bauer, G. Electronic structure of $PbTe/Pb_{1-x}Sn_xTe$ superlattices. *Phys. Rev. B* **1984**, *30*, 3394−3405.
(39) Popescu, V.; Zunger, A. Extracting E versus $\vec{k}$ effective band structure from supercell calculations on alloys and impurities. *Phys. Rev. B* **2012**, *85*, 085201.
(40) McMillan, W. L. Transition temperature of strong-coupled superconductors. *Phys. Rev.* **1968**, *167*, 331−344.

https://doi.org/10.1021/acs.nanolett.2c02422
Nano Lett. XXXX, XXX, XXX−XXX

(41) Allen, P. B.; Dynes, R. C. Transition temperature of strong-coupled superconductors reanalyzed. *Phys. Rev. B* **1975**, *12*, 905−922.
(42) Giustino, F. Electron-phonon interactions from first principles. *Rev. Mod. Phys.* **2017**, *89*, 015003.
(43) Poncé, S.; Margine, E. R.; Verdi, C.; Giustino, F. EPW: Electron−phonon coupling, transport and superconducting properties using maximally localized Wannier functions. *Comput. Phys. Commun.* **2016**, *209*, 116−133.
(44) Liu, Y.; Wang, Z.; Zhang, X.; Liu, C.; Liu, Y.; Zhou, Z.; Wang, J.; Wang, Q.; Liu, Y.; Xi, C.; Tian, M.; Liu, H.; Feng, J.; Xie, X. C.; Wang, J. Interface-induced Zeeman-protected superconductivity in ultrathin crystalline lead films. *Phys. Rev. X* **2018**, *8*, 021002.
(45) Klemm, R. A.; Luther, A.; Beasley, M. Theory of the upper critical field in layered superconductors. *Phys. Rev. B* **1975**, *12*, 877−891.
(46) Tinkham, M. *Introduction to superconductivity*, 2nd ed.; Dover Publications: New York, 2004.
(47) Zhang, J.; Zhang, S.; Weng, H.; Zhang, W.; Yang, L.; Liu, Q.; Feng, S.; Wang, X.; Yu, R.; Cao, L.; Wang, L.; Yang, W. G.; Liu, H. Z.; Zhao, W. Y.; Zhang, S.-C.; Dai, X.; Fang, Z.; Jin, C. Q. Pressure-induced superconductivity in topological parent compound Bi_2Te_3. *Proc. Natl. Acad. Sci. U.S.A.* **2011**, *108*, 24−28.
(48) Kohulak, O.; Martoňák, R.; Tosatti, E. High-pressure structure, decomposition, and superconductivity of MoS_2. *Phys. Rev. B* **2015**, *91*, 144113.
(49) Fu, L.; Wan, Y.; Tang, N.; Ding, Y.-m.; Gao, J.; Yu, J.; Guan, H.; Zhang, K.; Wang, W.; Zhang, C.; Shi, J.-j.; Wu, X.; Shi, S.; Ge, W.; Dai, L.; Shen, B. K-Λ crossover transition in the conduction band of monolayer MoS_2 under hydrostatic pressure. *Sci. Adv.* **2017**, *3*, No. e1700162.
(50) Liu, L.; Yang, H.; Huang, Y.; Song, X.; Zhang, Q.; Huang, Z.; Hou, Y.; Chen, Y.; Xu, Z.; Zhang, T.; Wu, X.; Sun, J.; Huang, Y.; Zheng, F.; Li, X.; Yao, Y.; Gao, H.-J.; Wang, Y. Direct identification of Mott Hubbard band pattern beyond charge density wave superlattice in monolayer 1*T*-$NbSe_2$. *Nat. Commun.* **2021**, *12*, 1978.
(51) Luo, H.; Xie, W.; Tao, J.; Inoue, H.; Gyenis, A.; Krizan, J. W.; Yazdani, A.; Zhu, Y.; Cava, R. J. Polytypism, polymorphism, and superconductivity in $TaSe_{2-x}Te_x$. *Proc. Natl. Acad. Sci. U.S.A.* **2015**, *112*, E1174−E1180.
(52) Sun, K.; Sun, S.; Zhu, C.; Tian, H.; Yang, H.; Li, J. Hidden CDW states and insulator-to-metal transition after a pulsed femtosecond laser excitation in layered chalcogenide 1T-$TaS_{2-x}Se_x$. *Sci. Adv.* **2018**, *4*, No. eaas9660.
(53) Li, Y.; Gu, Q.; Chen, C.; Zhang, J.; Liu, Q.; Hu, X.; Liu, J.; Liu, Y.; Ling, L.; Tian, M.; Wang, Y.; Samarth, N.; Li, S.; Zhang, T.; Feng, J.; Wang, J. Nontrivial superconductivity in topological $MoTe_{2-x}S_x$ crystals. *Proc. Natl. Acad. Sci. U.S.A.* **2018**, *115*, 9503−9508.
(54) Yan, D.; Wang, S.; Lin, Y.; Wang, G.; Zeng, Y.; Boubeche, M.; He, Y.; Ma, J.; Wang, Y.; Yao, D.-X.; Luo, H. NbSeTe—a new layered transition metal dichalcogenide superconductor. *J. Phys.: Condens. Matter* **2020**, *32*, 025702.
(55) Yang, F.; Miao, L.; Wang, Z.; Yao, M.-Y.; Zhu, F.; Song, Y.; Wang, M.-X.; Xu, J.-P.; Fedorov, A. V.; Sun, Z.; Zhang, G. B.; Canhua, L.; Liu, F.; Qian, D.; Gao, C. L.; Jia, J.-F. Spatial and energy distribution of topological edge states in single Bi(111) bilayer. *Phys. Rev. Lett.* **2012**, *109*, 016801.
(56) Drozdov, I. K.; Alexandradinata, A.; Jeon, S.; Nadj-Perge, S.; Ji, H.; Cava, R.; Andrei Bernevig, B.; Yazdani, A. One-dimensional topological edge states of bismuth bilayers. *Nat. Phys.* **2014**, *10*, 664−669.
(57) Reis, F.; Li, G.; Dudy, L.; Bauernfeind, M.; Glass, S.; Hanke, W.; Thomale, R.; Schäfer, J.; Claessen, R. Bismuthene on a SiC substrate: A candidate for a high-temperature quantum spin Hall material. *Science* **2017**, *357*, 287−290.
(58) Kezilebieke, S.; Huda, M. N.; Vaňo, V.; Aapro, M.; Ganguli, S. C.; Silveira, O. J.; Głodzik, S.; Foster, A. S.; Ojanen, T.; Liljeroth, P. Topological superconductivity in a van der Waals heterostructure. *Nature* **2020**, *588*, 424−428.
(59) Rosenzweig, P.; Karakachian, H.; Marchenko, D.; Küster, K.; Starke, U. Overdoping graphene beyond the van Hove singularity. *Phys. Rev. Lett.* **2020**, *125*, 176403.

https://doi.org/10.1021/acs.nanolett.2c02422
Nano Lett. XXXX, XXX, XXX−XXX